Case Studies in Construction Materials 6 (2017) 16–28

Contents lists available at ScienceDirect

Case Studies in Construction Materials

journal homepage: www.elsevier.com/locate/cscm

Short communication

Mechanical characterization of the structural components of Pre-Columbian earthen monuments: Analysis of bricks and mortar from Huaca de la Luna in Perú

Rafael Aguilar[a,*], Mijaíl Montesinos[a], Santiago Uceda[b]

[a] Department of Engineering, Civil Engineering Division, Pontificia Universidad Católica del Perú PUCP, Av. Universitaria 1801, San Miguel, Lima 32, Perú

[b] Department of Archaeology and Anthropology, National University of Trujillo, Trujillo, Perú

ARTICLE INFO

Article history:
Received 2 September 2016
Accepted 14 November 2016
Available online 17 November 2016

Keywords:
Archaeological heritage
Earthen buildings
Bricks and mortar
Mechanical characterization

ABSTRACT

The paper deals with the mechanical characterization of the materials that composes the structural system of the archaeological earthen complex of 'Huaca de la Luna' in Perú (100–900A.D.). The mechanical characterization was carried out through uniaxial compression, three-point bending and splitting tests. The results indicate differences in bricks and mortar samples in strength capacity and elastic stiffness in compression, as well as differences in rupture modulus and diametric compression strength. The study contributes to understand the linear and nonlinear behavior of archaeological earthen materials and structures and provides reference values for the structural assessment of similar buildings and monuments.

1. Introduction

Earth had been used by many ancestral civilizations as a construction material. In the region of modern Perú, the oldest evidence of use of earth dates back to approximately 2600 B.C. [1]. The 'Huacas' are the oldest earthen construction typology in Perú; they are massive pyramidal structures of religious character. These edifications were built with different types of constructive systems such as adobe masonry with unfired mud bricks and mortar, as well as rammed earth. Many of these earthen pyramids have been found at archeological sites along the coastal region of Perú. Unfortunately, this geographic location makes these structures vulnerable to a wide range of natural hazards such as earthquakes (Perú is located within the Pacific subduction zone and the Pacific Ring of Fire), erosion due to wind and heavy rains, as well as rainfall induced landslides due to the recurring weather phenomenon of El Niño. In fact, archeological evidences show that many ancestral cultures in Perú were heavily affected, or even devastated, due to the action of one or more of these hazards [2].

The present paper analyzes the mechanical properties of the adobe bricks and earthen mortar that composes the structural system of the most important and best preserved 'Huaca' in Perú, Huaca de la Luna, and is carried out as part of a broad seismic assessment program in progress. As shown in Fig. 1, Huaca de la Luna is a massive earthen complex that correspond to the peak development moment of the Moche civilization. The monument had several sectors built in different kingdoms from 100 A.D. to 900 A.D. (Fig. 1a). Huaca de la Luna had been covered with eolian sand but was recently

* Corresponding author.
E-mail address: raguilar@pucp.pe (R. Aguilar).

http://dx.doi.org/10.1016/j.cscm.2016.11.003

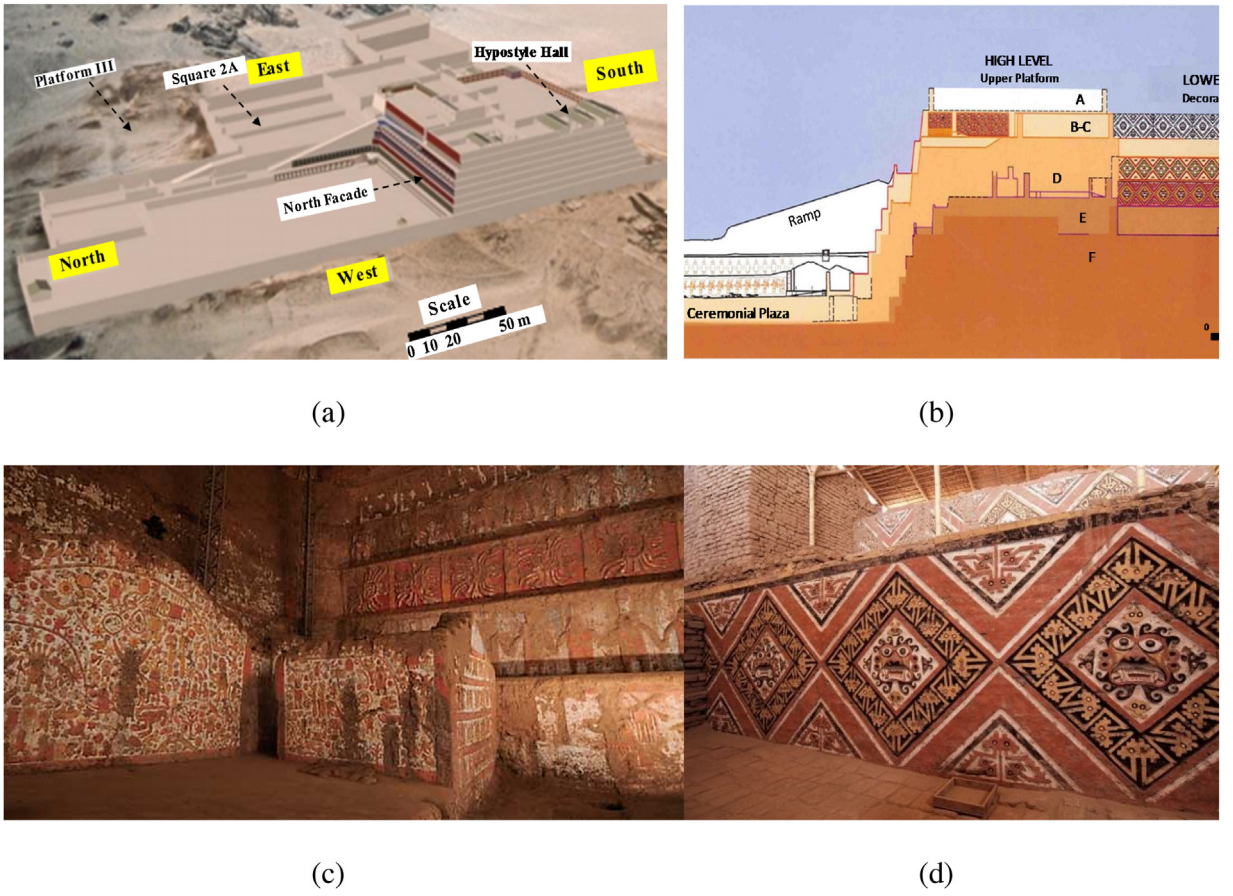

Fig. 1. Huaca de la Luna: (a) hypothetical reconstruction of Huaca de la Luna in 900A.D. [adapted from 5]; (b) section view with construction sequence of the monument [5]; (c) artistic details at the north façade; and (d) artistic details in the interior of the monument.

discovered at the beginning of the 90s. According to [3], the construction of the main pyramid consisted on the overlapping of at least six stages (see Fig. 1b). It is believed that the reason for this type of sequential construction is based on the idea of renewal of power corresponding to the start of a new ruler [3,4]. Examples of some of the impressive artistic features that include high relief and colorful surfaces with different motives can be seen in Fig. 1c and d.

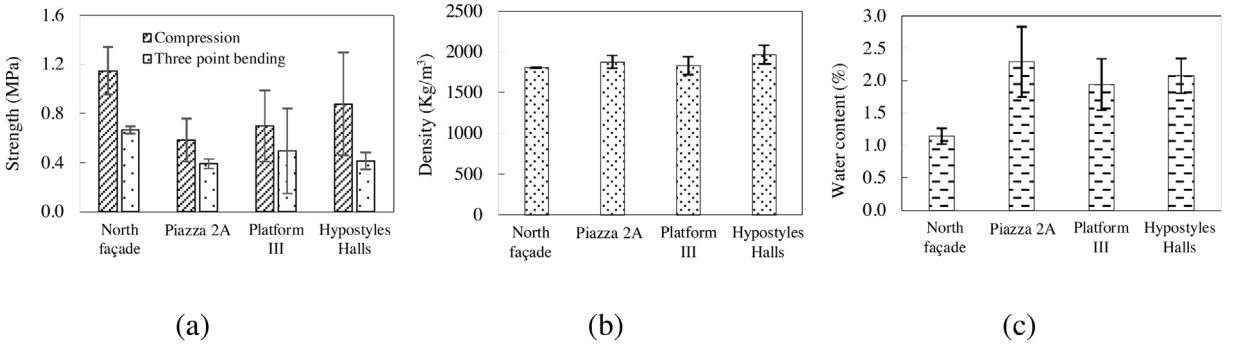

Fig. 2. Summary of literature review of previous mechanical tests in adobe bricks of Huaca de la Luna [adapted from 6]: (a) compression and three-point bending characterization; (b) density measurements; and (c) water content measurements.

2. Material description

The present paper focuses on the mechanical characterization of adobe bricks and earthen mortar that conforms the structural system of a recent discovered and latest built sector at Huaca de la Luna: 'Templo Nuevo'. As shown in Fig. 3a, the sector 'of Templo Nuevo' was built on the northeast side of the archaeological complex around the 10th Century A.D. [3].

2.1. Previous studies

The archaeologists in charge of the Project Huaca de la Luna are carrying out historical, archaeological and material investigations on the monument for more than 25 years. As shown in [5] these studies aimed at the characterization of the strength capacity of adobe bricks from the main pyramid. Fig. 2a summarizes the reported results to uniaxial compression and three-point bending tests corresponding to the following sectors: North facade, Square 2a, Platform III, and Hypostyle Hall (see locations in Fig. 1a). As shown in Fig. 2, it was found that the maximum strength to uniaxial compression (defined as the ratio between the maximum load registered and the transversal area of the tested specimens) varied within a range of 0.49 MPa–1.36 MPa. For the case of the rupture modulus (calculated as the relation between maximum force and geometrical properties in three-point bending tests), the results evidence variations in a range of 0.19 MPa–0.86 MPa. As seen on Fig. 2b, the results of density show less variability from the different sectors with maximum and minimum values of 1700 kg/m3 and 2080 kg/m3, respectively. For the case of the humidity content (Fig. 2c), the results indicate minimum and maximum values of 1.06 % and 2.91 %, respectively.

2.2. Samples extraction and preliminary classification

For the present work, 80 bricks and 250 kg of mortar were extracted from the sector of 'Templo Nuevo' and transported overland to the laboratory of structures at PUCP in Lima. Fig. 3b and c show the extraction process of bricks and mortar. As shown, the extraction was carefully carried out by specialized personal. The extracted samples were immediately covered by plastic films and then stored in wooden boxes with internal foam isolation (Fig. 3d). Fig. 3e shows the stored boxes in the laboratory.

Once the material arrived to the laboratory, the variability of dimensions of the bricks was analyzed through geometrical measurements in different sections of each unit (see Fig. 4a). As shown in Fig. 4b–d, the bricks presented high geometrical variability due to wind erosion and perhaps a non-controlled fabrication process. The average dimensions of the bricks were of 320 mm length, 220 mm width, and 120 mm height.

A subsequent analysis of material homogeneity was carried out in the bricks using 2D tomography from direct Ultrasonic Pulse Velocity (UPV) tests, as suggested by [7] As shown in Fig. 5a, the 2D tomography was the result of P-wave velocity

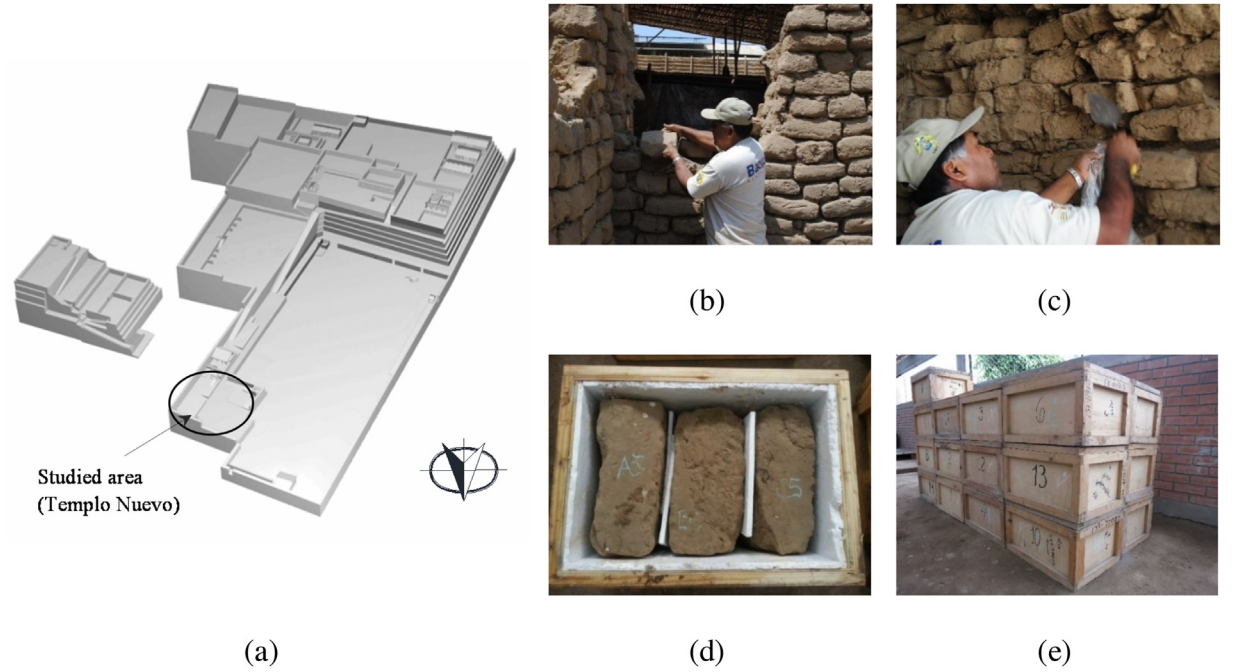

Fig. 3. Material extraction process: (a) studied sector; (b) extraction process of adobes; (c) extraction process of mortar; (d) adobes in boxes; and (e) boxes storing at the laboratory.

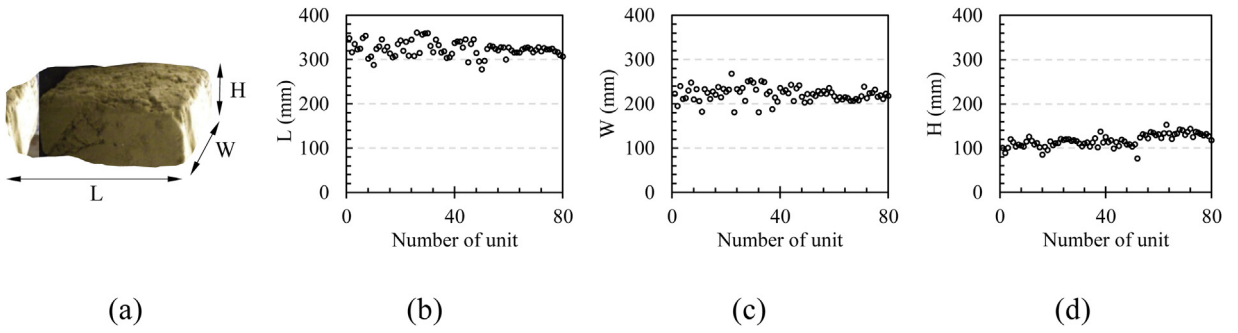

Fig. 4. Dimensional variability analysis of adobe bricks: (a) schematic view of a brick; (b) length results; (c) width results; and (d) height results.

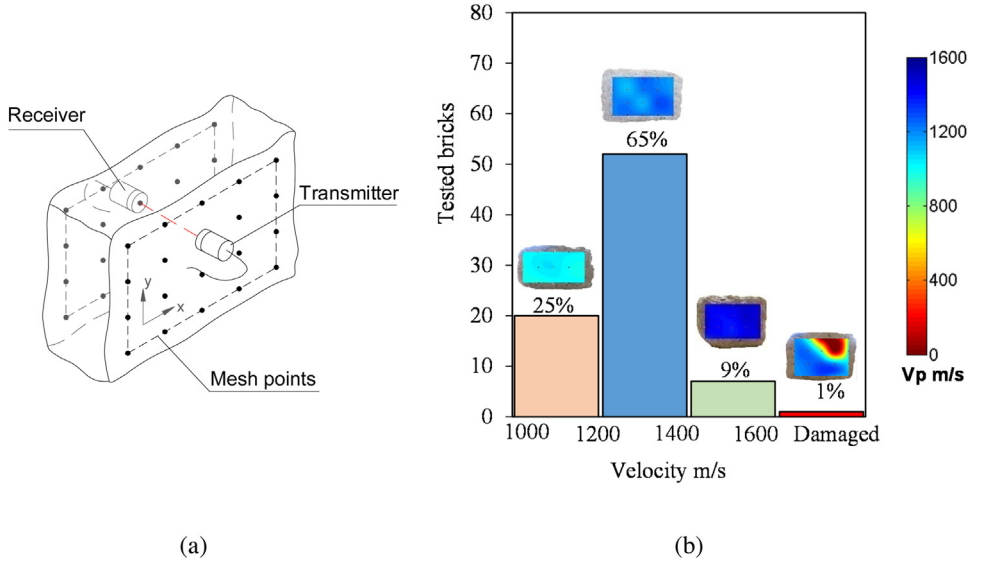

Fig. 5. Homogeneity analysis for the bricks: (a) 2D tomography test setup; and (b) results of variability in P-wave velocities.

records in the nodes of grids defined for each brick in function of their geometry. Given the different dimensions of the bricks, three types of grid sizes were used, namely Type I (65 mm × 60 mm), Type II (60 mm × 50 mm) and Type III (60 mm × 60 mm). One transmitter and one receiver were used for the UPV tests and the transmitter velocity was set to 54 KHz. The maximum P-wave velocity registered during the tests was of 1650 m/s and the minimum of 900 m/s. As shown in Fig. 5b, the majority (99%) of the bricks evidenced a homogenous conformation and only one brick evidenced damage in one of its corners. As observed, the P-wave velocity of 65% of the bricks ranged from 1200 to 1400 m/s, while 25% of the bricks had P-wave velocities ranging from 1000 to 1200 m/s. Only few bricks (9%) presented velocities higher than 1400 m/s. The reduced variability of velocities on groups of bricks may indicate some kind of standardization during the material selection and the fabrication process.

Table 1
Density and water content results for the tested adobe bricks and mortar.

		Density (Kg/m^3)	Water content (%)
Brick	Average	1758	1.9
	CV	2%	14%
Mortar	Average	1984	3.6
	CV	7%	14%

2.3. Physical characterization

The physical characterization of the bricks and mortar material was carried out though the determination of densities and water contents according to ASTM D7263 [8] and ASTM D4643 [9], respectively. Granulometric analysis and determination of plasticity limits was also carried out following the recommendations of ASTM D422 [10] and ASTM D4318 [11], respectively.

For bricks analyses, four samples from the most representative group (P-wave velocity ranging from 1200 m/s to 1400 m/s) were selected to determine density and water content. To study the mortar density and water content, eighteen samples were randomly chosen representing approximately 20 kg of soil. As observed in Table 1, the average density of bricks (1758 kg/m3) is 12% lower than the average density of the mortar (1984 kg/m3) and the Coefficient of Variation (CV) of these measurements are very low (less than 10%). The registered water content values for the bricks and mortar was of 1.9% and 3.6%, respectively with slightly higher CV.

The granulometric characterization and plasticity limit determination was carried out with pieces of bricks and mortars which represented approximately 850 gr of gross soil in each case. Fig. 6 presents the granulometric results together with envelope curves corresponding to the values reported in [12] and [6] from the material of the main pyramid. As shown in Fig. 6a, the values for bricks indicate similar composition in terms of larger particles. In the silt and clay region, it is clear that the soil samples present finer particles. No values were registered for plasticity limits indicating sand predominance. With these considerations, the brick soil was classified as Sandy Loam Soil SM according to ASTM D2487 [13]. For what respects to the mortar results (Fig. 6b), the curve evidence again presence of high quantities of fine particles (in opposition to what was found for the main pyramid in previous studies – see envelope curve). The liquid and plastic limits were of 25% and 15%, respectively. With these considerations, the mortar soil was classified as a Low Plasticity Clay Soil CL according to ASTM D2487 [13].

3. Experimental program for the mechanical characterization to uniaxial compression, flexure and tension

3.1. Testing procedure

The mechanical characterization consisted on the study of the behavior of bricks and mortar subjected to uniaxial compression, three-point bending and splitting loads. All the tests were carried out with a Zwick/Roell Z050 universal testing machine and the loads were applied with displacement control (see setup in Fig. 7a). For the uniaxial compression tests, the Australian standard [14] and ASTM C469 [15] were taken as a reference. Also the recommendations from [16] and [17] were taken into account to perform this test. The displacement velocity of the load frame was set to 0.5 mm/min. The displacements of the load cell were recorded in all tests, and its measurements were considered as the global deformation of the specimens (see Fig. 7b). Localized deformations in the middle third of the specimens were measured using a Digital Image Correlation (DIC) technique which was carried out through an ARAMIS 5M system [18] with a strain precision of 0.005%. For the three-point bending tests (Fig. 7c), the considerations proposed by the Australian Standard [14] were taken into account. Finally, the technical recommendations of the RILEM CPC 6 [19] were used for the splitting tests. The load velocity was 0.25 mm/min for the three-pint bending and splitting tests. DIC was also used to assess the strain evolution in the three-point bending tests. The referred standards for compression, three-point bending and splitting tests were taken only as guidelines and not rigorously followed given the fact that there is no specific information for testing archaeological material.

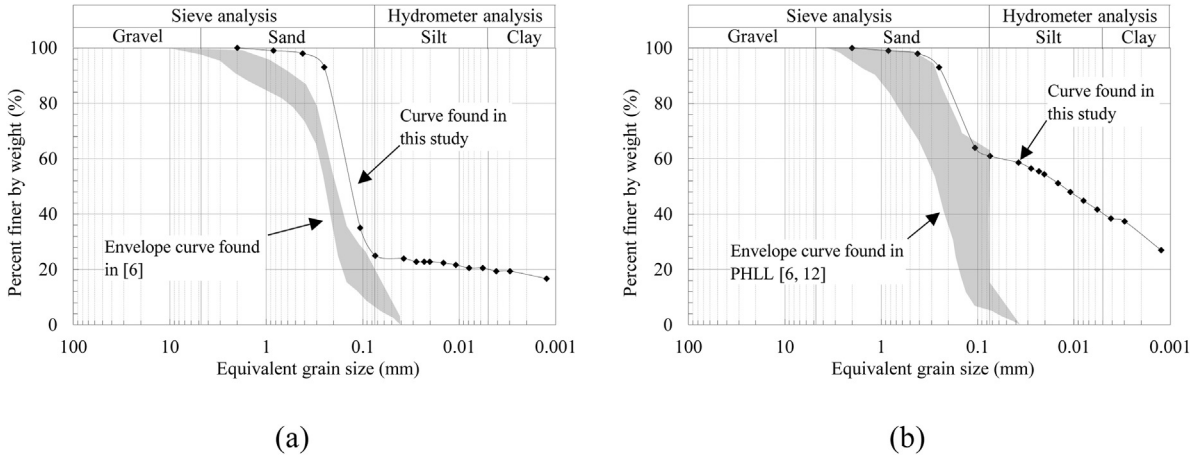

Fig. 6. Granulometric characterization results: (a) curves for bricks; and (b) curves for mortar.

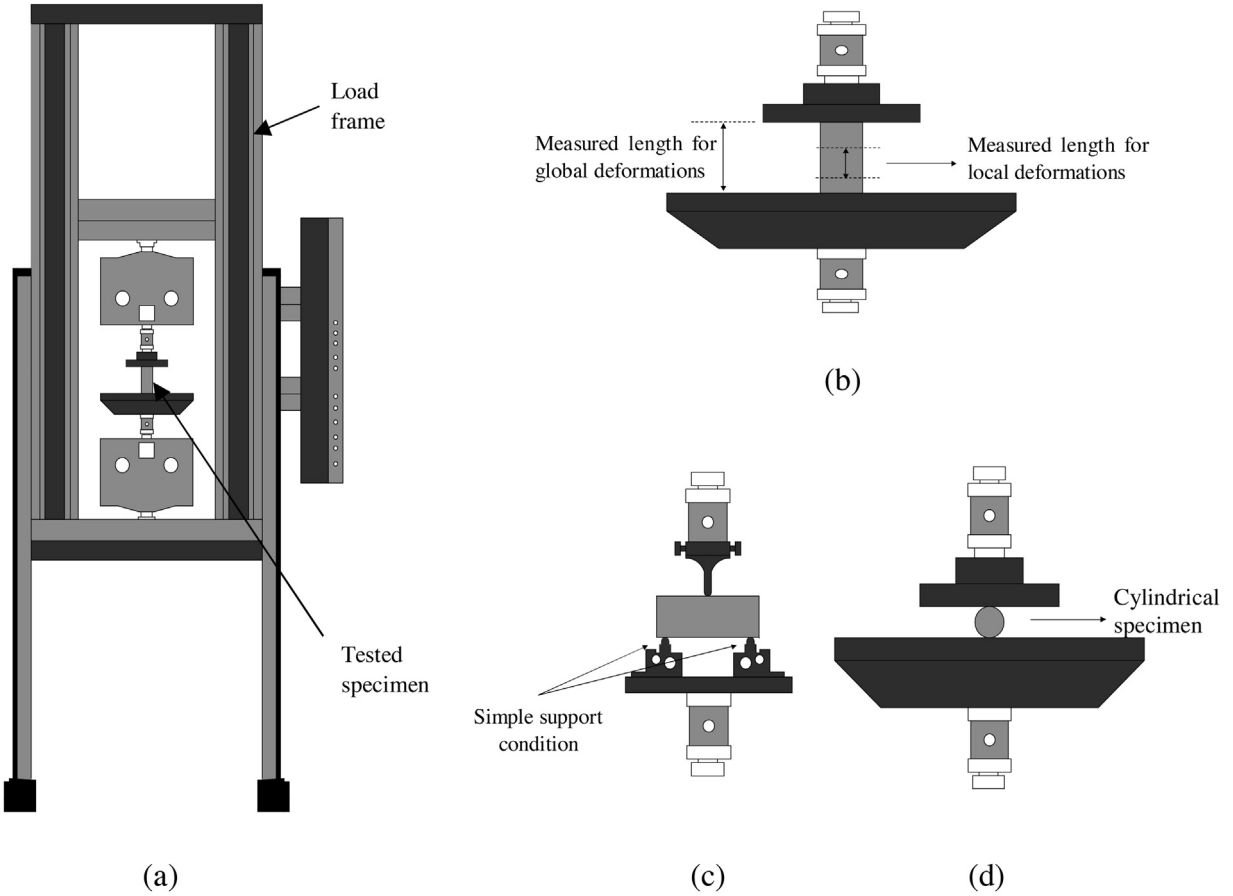

Fig. 7. Testing setup: (a) universal loading machine; (b) uniaxial compression test; (b) three-point bending test; and (c) splitting test.

3.2. Samples preparation

For the characterization to uniaxial compression, prismatic specimens of 45 mm width, 45 mm thickness and 120 mm of height were prepared (in case of the bricks samples, the height coincided with the height of the original brick). Four bricks (one of them is shown in Fig. 8a) were selected and these corresponded to the most representative group as defined in the previous section (P wave velocity ranging from 1200 m/s to 1400 m/s). As shown in Fig. 8b and Fig. 8c, the original bricks were sawed obtaining 24 prismatic elements for testing. On the other hand, for the mortar, 21 prismatic samples were fabricated remixing triturated soil which was previously left for curing 24 h in water under saturated condition before casting (see Fig. 8d). The resulting mud was placed into prismatic formworks (Fig. 8e) and dried in environmental conditions for approximately 30 days. The final samples are shown in Fig. 8f.

For the characterization to three-point bending, 12 prismatic specimens were prepared following the same fabrication procedure used in the uniaxial compression tests for the bricks and the mortar. In this case, adobe specimens had average cross section of 43 mm $\times$ 44 mm and lengths varying from 110 mm to 160 mm. For the mortar, 10 specimens were fabricated with similar average cross section than the bricks specimens while the lengths varied from 100 mm to 240 mm.

For the characterization to splitting, cylindrical specimens (Fig. 8f) were fabricated using triturated soil for both, bricks and mortars. As in the previous cases, the fabrication process considered a drying time of approximately 30 days under environmental conditions. With all these considerations, 9 cylindrical specimens with average diameter of 34 mm and 96 mm of height were fabricated for the characterization of bricks. For the mortar, 20 specimens were fabricated with average diameter of 34 mm and 74 mm of height.

Table 2 shows the summary of the experimental program for the uniaxial compression, three-point bending and splitting tests.

Fig. 8. Samples preparation for mechanical characterization: (a) original adobe brick; (b) sawing process of adobe bricks; (c) prismatic specimens for compression and flexure in adobe; (d) remixing process for the preparation of mortar specimens; (e) mortar on formwork; and (f) specimens for compression and flexure tests of mortar and splitting tests of adobe and mortar.

Table 2
Number of tested samples for the mechanical characterization.

	Performed test	Type of sample	No of tested specimens
Brick	Compression	Prismatic	24
	Three point bending	Prismatic	12
	Splitting	Cylinder	9
Mortar	Compression	Prismatic	21
	Three point bending	Prismatic	10
	Splitting	Cylinder	20

4. Uniaxial compression tests results and discussion

4.1. Stress-strain curves

Based on the load history and the strains obtained during the uniaxial compression tests, the stress-strain curves that characterize the behavior of bricks (Fig. 9) and mortar (Fig. 10) were obtained. The uniaxial compressive strength (f_c) of the bricks and mortar were obtained as the ratio between the maximum loads registered during the tests and the initial transversal area of the specimens. In both cases, the construction of two set of curves was considered: the first one considering the strains calculated from the displacement measurements of the load cell (denoted here as global measurements), and the second one considering the strains measured in the middle third of the specimens with DIC (denoted here as local measurements). As shown, both bricks and mortar presented a quasi-brittle behavior for compression.

Fig. 11a and b compare the results in terms of envelopes of stress-strain curves obtained for the adobe and mortar, respectively. As shown, in both cases, significant differences can be found when comparing stress-strain relationships built with global and local deformation measurements. In the elastic region of the curve, it is clear the presence of an initial contact adjustment phase in all the global records. There is also a clear difference of strain levels at the peak strength. The inelastic region also presents differences in ultimate strain levels; global measurements evidence higher values than local measurements.

Table 3 summarizes the results of the uniaxial compression tests considering a statistical filter using the Interquartile Range (*IQR*) criterion defined as the difference between the third (Q_3) and first quartile (Q_1) to discard outliers (lower and

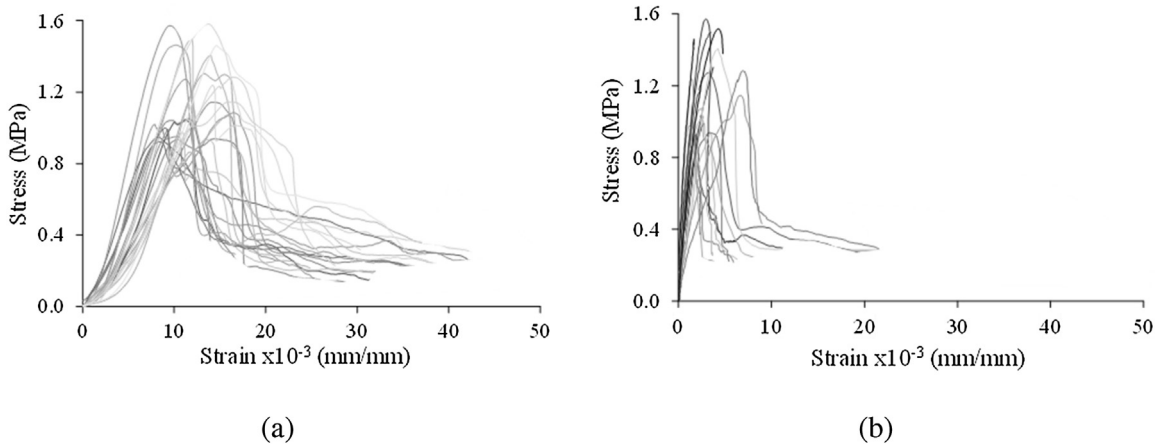

Fig. 9. Stress-strain results for bricks tested under uniaxial compression: (a) data set results calculated with global deformation measurements; and (b) data set results calculated with local deformation measurements.

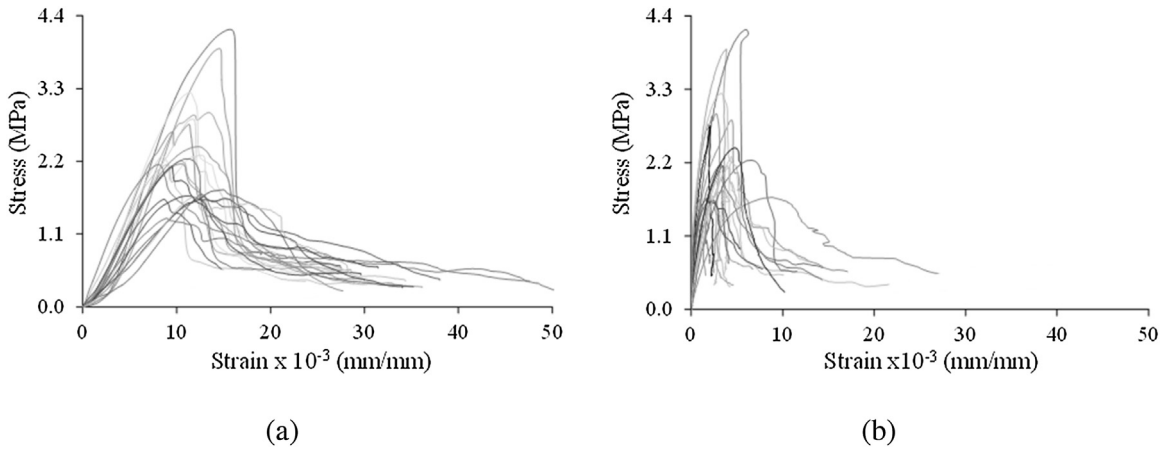

Fig. 10. Stress-strain results for mortar tested under uniaxial compression: (a) data set results calculated with global deformation measurements; and (b) data set results calculated with local deformation measurements.

upper outliers were the values below $Q_1 - 1.5IQR$ and above $Q_3 + 1.5IQR$, respectively). The brick results show an average f_c of 1.16 MPa with a CV of 21%. In case of the mortar, the average f_c was 2.33 MPa with a CV of 32%. These results indicate that the compressive strength of the bricks is lower than the mortar which might be due to differences in soil type and the influence of the sample preparation process. The strains calculated at the peak stress (ε_c) show similar values for bricks and mortar (when comparing corresponding values of ε_c local and ε_c global in each case). The ε_c results also show that global deformation measurements can provide values in a range of 3.4– 3.9 times higher than local deformation measurements. A comparison of Elasticity Modulus (E-modulus) was also carried out from the stress-strain curves results and for that global (E_{global}) and local (E_{local}) measurements were taken into account. For global deformation measurements, E_{global} corresponds to the secant elasticity modulus calculated considering the 30% f_c and 60% f_c, as suggested by [20]. In the case of local deformation measurements, E_{local} corresponds to the secant E-modulus calculated considering the zero stress point and 33% f_c, as suggested by [21]. The results of E-modulus show that the mortar is approximately twice higher than the bricks confirming differences in the material. These results also indicate that the E values calculated with local deformation measurements can result in approximately six times higher values when compared to the calculated from global deformation measurements. This difference might be attributed to the influence of the boundary conditions in the global measurements, as suggested by [22].

Based on the local strain-stress curves, compression constitutive laws that represent the behavior of bricks and mortar were finally proposed. For this, stress and strain results were normalized with respect to the results at peak strength. Fig. 12 shows the proposed theoretical curves and its comparison to the experimental results. For the elastic region (Eq. (1) and Eq. (4)), the data was adjusted to the equation proposed by [23]. The inelastic region was represented by two sets of

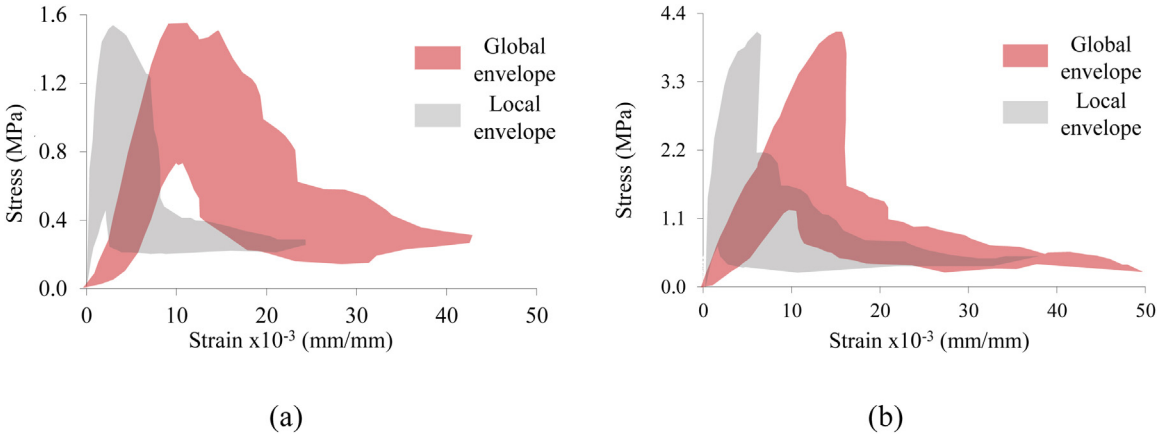

Fig. 11. Stress-strain results comparison: (a) brick results; and (b) mortar results.

relationships: first a natural logarithm decay until reaching the 20% of the compressive strength (Eq. (2) and Eq. (5)), and then a constant strength representing residual values (Eq. (3) and Eq. (6)).

Table 3
Summary of uniaxial compression tests results for bricks and mortar.

Analyzed material		f_c (MPa)	ε_{clocal} (10^{-3})	$\varepsilon_{cglobal}$ (10^{-3})	E_{local} (MPa)	E_{global} (MPa)
Brick	Average	1.16	3.16	12.40	801	147
	Standard deviation	0.25	1.63	2.76	333	40
	CV	21%	51%	22%	42%	27%
Mortar	Average	2.33	3.42	11.56	1835	293
	Standard deviation	0.75	1.44	2.09	940	92
	CV	32%	42%	18%	51%	32%

4.2. Failure analysis

The analysis of the failure of the specimens allowed understanding the influence of the load application, the crack propagation pattern, as well as the variability of resulting mechanical properties in the uniaxial compression tests. Fig. 13 shows an example of evolution of principal strains observed in one of the tests and the plot of the relationship of applied stress vs elapsed testing time corresponding to three typical failures. In this Figure, the values in brackets indicate load stage and the values in percentage indicate the relationship of stress and maximum strength. The values in parenthesis indicate the elapsed time from the beginning of the test. As observed in Fig. 13a, until approximately 60% f_c, the strain distribution indicates an elastic behavior in the specimen. At 63% f_c, strain concentrations start to be visible close to the top load plate. At 95% f_c, a small vertical crack appears in the bottom right corner of the specimen. At the maximum strength (100% f_c), the single vertical crack started to propagate. The post peak behavior (after 130 s) evidences a rapid crack propagation. A 5% f_c decrement (corresponding to results at 150 s) shows a severely cracked specimen. These cracks produce degradation of the specimen until reaching 20% f_c decrement (corresponding to results at 171 s). After this point the cracks only continue to open until the complete loss of strength at the end of the test. Fig. 13b evidences that the variability of the results is also dependent on the type of failure. Splitting failure are often fragile and provide unstable results while cone and diagonal failures may produce comparable stress-strain relationships.

5. Three-point bending and splitting tests results and discussion

5.1. Three-point bending tests

The measurement of the load history and vertical displacements of the load plate during the three-point bending tests allowed obtaining force-displacement relationships that characterized the behavior of bricks (Fig. 14a) and mortar (Fig. 14b). As shown, the results evidenced high variability in terms of registered maximum loads, as well as peak and ultimate

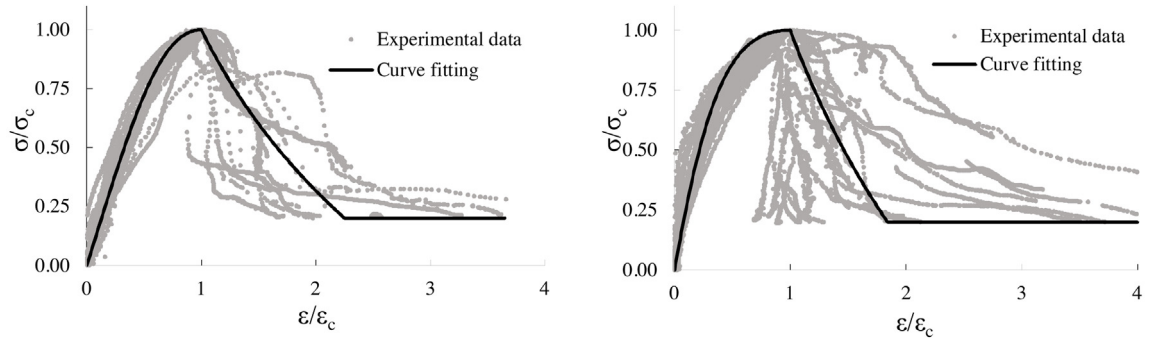

$$\frac{\sigma}{\sigma_c} = \frac{2.77\frac{\varepsilon}{\varepsilon_c}}{(2.77-1)+\left(\frac{\varepsilon}{\varepsilon_c}\right)^{2.77}} \qquad 0 \le \frac{\varepsilon}{\varepsilon_c} \le 1 \qquad \text{Equation (1)}$$

$$\frac{\sigma}{\sigma_c} = -\frac{\ln\left(\frac{\varepsilon}{\varepsilon_c}\right)}{1.015} + 1 \qquad 1 < \frac{\varepsilon}{\varepsilon_c} \le 2.25 \qquad \text{Equation (2)}$$

$$\frac{\sigma}{\sigma_c} = 0.2 \qquad 2.25 < \frac{\varepsilon}{\varepsilon_c} \qquad \text{Equation (3)}$$

(a)

$$\frac{\sigma}{\sigma_c} = \frac{1.61\frac{\varepsilon}{\varepsilon_c}}{(1.61-1)+\left(\frac{\varepsilon}{\varepsilon_c}\right)^{1.61}} \qquad 0 \le \frac{\varepsilon}{\varepsilon_c} \le 1 \qquad \text{Equation (4)}$$

$$\frac{\sigma}{\sigma_c} = -\frac{\ln\left(\frac{\varepsilon}{\varepsilon_c}\right)}{0.763} + 1 \qquad 1 < \frac{\varepsilon}{\varepsilon_c} \le 1.84 \qquad \text{Equation (5)}$$

$$\frac{\sigma}{\sigma_c} = 0.2 \qquad 1.84 < \frac{\varepsilon}{\varepsilon_c} \qquad \text{Equation (6)}$$

(b)

Fig. 12. Proposed constitutive laws under uniaxial compression for: (a) bricks; and (b) mortar.

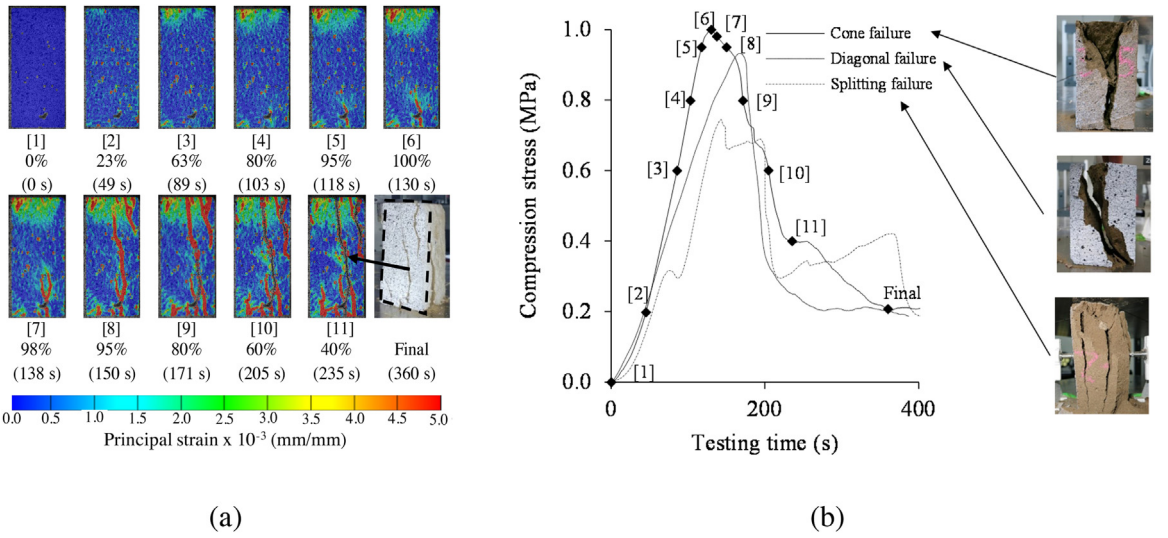

(a) (b)

Fig. 13. Crack propagation during uniaxial compression tests: (a) analysis of the evolution of cracking in time; and (b) stress vs elapsed time relationships associated to three types of failure.

displacements. Nevertheless, all the specimens presented a sudden failure just after reaching the maximum load which is expected due to the brittle nature of this material in tension.

The rupture modulus $\boldsymbol{f_b}$ (maximum strength in bending) of the bricks and mortar was then calculated using the relationship shown in Eq. (7), as proposed by [24]. In this Equation, $\boldsymbol{F}_{max}$ denotes the maximum force applied, and L, W and H are the length, width and height of the tested specimens, respectively.

$$f_b = \frac{3F_{max}L}{2WH} \qquad \text{Equation (7)}$$

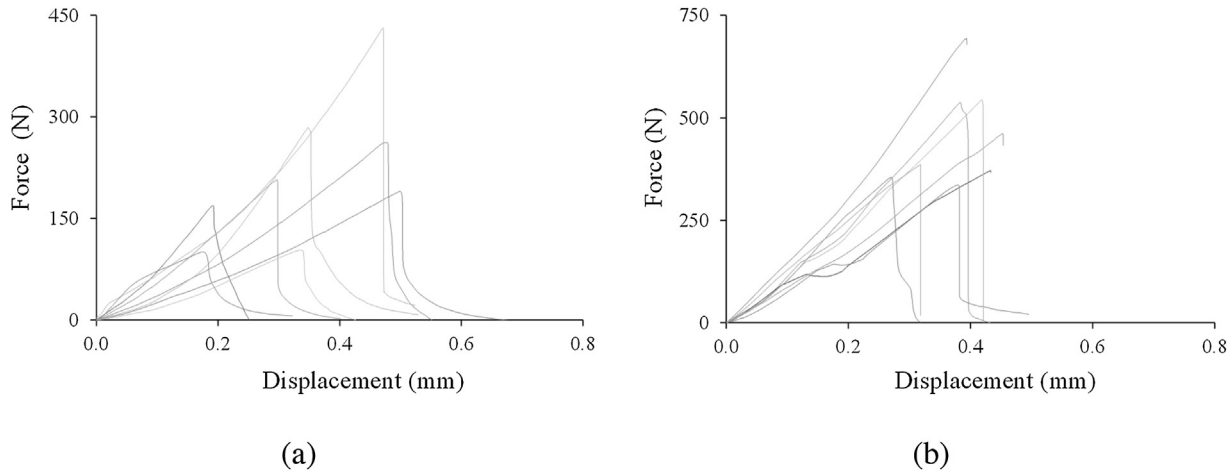

Fig. 14. Force vs mid-span vertical displacement results in the three-point-bending tests for: (a) bricks; and (b) mortar.

Table 4
Summary of three-point bending tests results for bricks and mortar.

Analyzed material		f_b (MPa)
Brick	Average	0.58
	Standard deviation	0.21
	CV	36%
Mortar	Average	1.11
	Standard deviation	0.32
	CV	29%

Table 4 summarizes the mechanical properties of brick and mortar obtained by the three-point bending tests. Again, to find more representative values, the *IQR* criterion was used to discard outlier values. As shown, bricks reached an average f_b of 0.58 MPa with a CV of 36%, while the mortar 1.11 MPa with a CV of 29%. These results confirm the existence of differences in both materials.

The overall evolution of the cracking pattern in the three-point bending tests for bricks and mortar was similar. Fig. 15a shows the cracking evolution in terms of strains for one of the tested brick specimens. As shown, the specimen remained linear until 92% f_b (at 89 s) where a first vertical crack appears at the mid span. This cracks propagates very fast (in the next 4s) until 100% f_b. A sudden loss of approximately 44% f_b is registered after 1.5 s and from that point on, the degradation of force capacity is slower but permanent until collapse. Fig. 15b shows force vs elapsed testing time relationships for two typical types of failures found in the tests: bending failure (the one that occur at the mid-span of the length) and shear failure (occurring close to one of the supports of the specimen). The influence of the type of failure in the maximum force capacity during tests is evident which is certainly one of the causes for variability in the registered results. Nevertheless, both results confirm a typical exponential decay of the specimens in the post peak region.

5.2. Splitting tests

Splitting tests were carried out to have a preliminary assessment of tensile strength of bricks and mortar. For comparison purposes, force vs load plate displacement curves are presented in Fig. 16. These results evidence consistency with very low dispersion of the registered rupture loads in the tests. As in compression and three-point bending, mortar specimens evidence higher resistance than the bricks.

With the records of applied maximum force (F_{max}) as well as the length (L) and the diameter (d) of the specimens, the diametric compression strength f_s for bricks and mortar was calculated using Eq. (8), as suggested in [15].

$$f_s = \frac{2F_{max}}{\pi L d} \qquad \text{Equation (8)}$$

Table 5 summarizes the results of the splitting tests (the *IQR* criterion was used to discard outliers and find more representative values). As observed, the average diametric compression strength registered for bricks and mortars were of 0.25 MPa and 0.38 MPa, respectively with reasonably low CV in both cases.

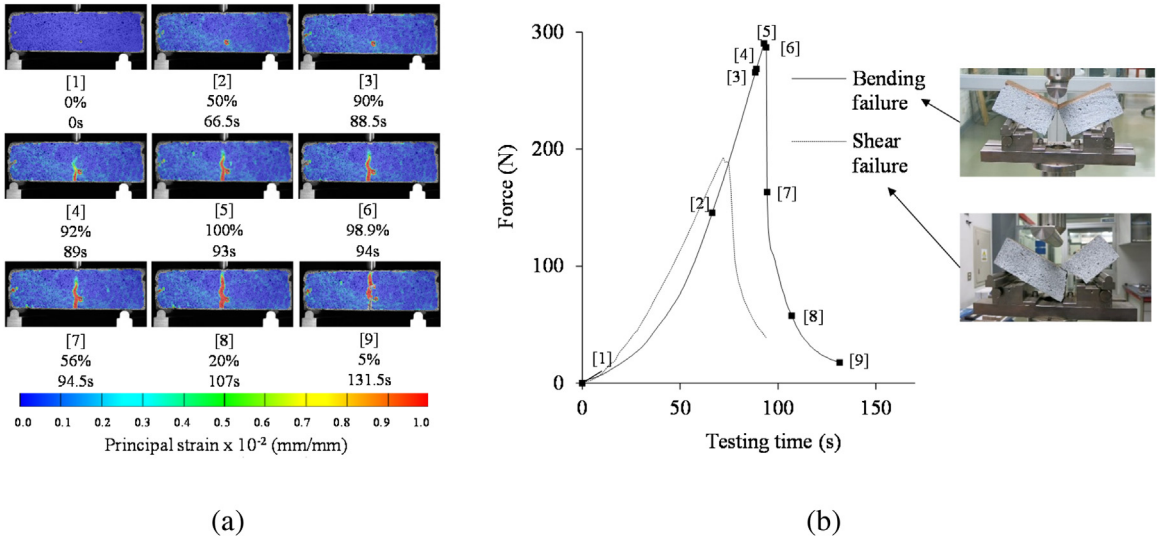

Fig. 15. Crack propagation during three-point bending tests: (a) analysis of the evolution of cracking in time; and (b) stress vs elapsed time relationships associated to two types of failure.

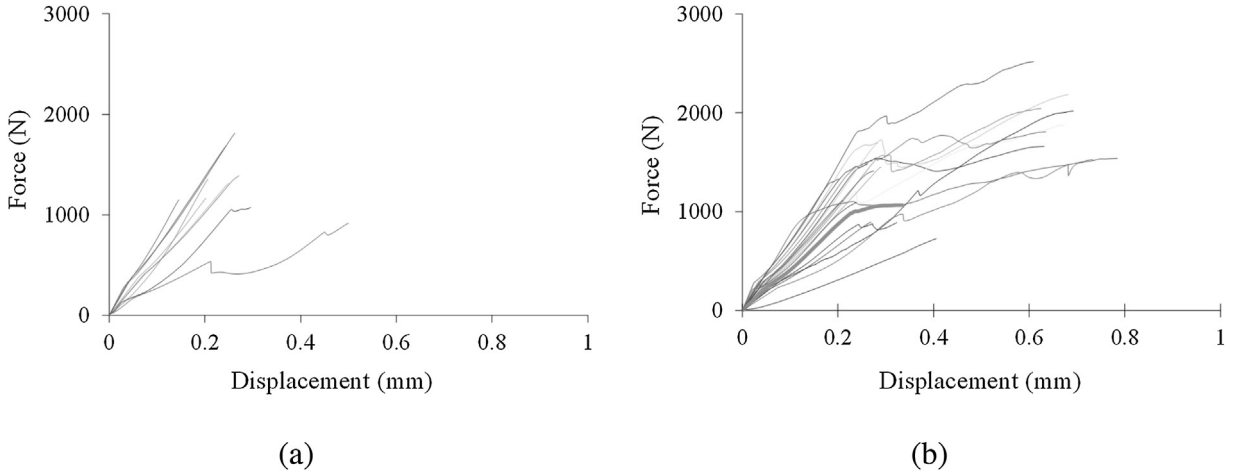

Fig. 16. Force vs vertical displacement results in the splitting tests: (a) adobe bricks; and (b) mortar.

6. Conclusions

The present paper deals with the mechanical characterization of the structural components of a millenarian massive earthen structure in Perú. Uniaxial compression, three-point-bending and splitting tests were carried out in prismatic and cylindrical samples of original adobe bricks and mortar of one of the recently discovered sectors of the monument.

Table 5
Summary of splitting tests results for bricks and mortar.

Analyzed material		f_s (MPa)
Brick	Average	0.25
	Standard deviation	0.06
	CV	23%
Mortar	Average	0.38
	Standard deviation	0.09
	CV	25%

The results of the performed tests evidence differences in the material of the bricks and mortar. The physical characterization show that the bricks are composed by silty sands while the mortar are clays with low plasticity. In terms of uniaxial compressive strength, the bricks have approximately 50% of the strength capacity of the mortar. The E-modulus results evidence also that the mortar is at least twice stiffer than the bricks. Contrarily, deformation results indicate similar values at peak strength as well as comparable ductility for bricks and mortar. In terms of rupture modulus, the results evidence differences of around 52% for the bricks and mortar samples. The diametric compression strength results show brick values of around 62% in correspondence to the mortar. These mechanical properties variations might be due to two reasons: actual differences in material (confirmed also by the physical tests), and aging considering that the bricks were original 100–900 AD. samples while the mortars were remixed in laboratory.

The failure analysis and stress-strain results of uniaxial compression tests confirm high variability of the material and also sensitivity to testing details such as the boundary conditions. Changes in this variable may originate initial strain concentrations which can also have influence in the final failure of the specimens. The results also evidence that the type of failure may govern the stress-strain behaviour inducing more variability in the testing results. To what respect to the failure analysis of the three-point bending tests, the results indicate also variability especially associated to the type of failure.

Acknowledgements

This research was carried out by the Engineering & Heritage Research Group at PUCP. The authors would like to acknowledge the Pontificia Universidad Católica del Perú PUCP and its funding office DGI-PUCP (project 89-2014) for providing funds to the project within which this work was developed. The authors would also like to thank the fellowship funding for postgraduate studies for the second author by CONCYTEC, PERU (Contract N° 012-2013-FONDECYT). The authors finally acknowledge the support of the Laboratory of Materials at PUCP for providing access to their facilities and equipment.

References

[1] R. Solis, J. Haas, W. Creamer, Dating Caral, a preceramic site in the Supe Valley on the central coast of Peru, Science 292 (5517) (2001) 723–726.
[2] R. Samanez, El terremoto que afectó al Cusco en 1950 y los aportes de George A. Kubler, Arkinka: revista de arquitectura, diseño y construcción 16 (204) (2012) 90–95.
[3] S. Uceda, A. Paredes, Arquitectura y función de la Huaca de la Luna, Revista Cultural des Indes 7 (1994) 42–46.
[4] S. Uceda, El poder y la muerte en la sociedad moche, in: L. Millones, M. Lemlij (Eds.), De Al Final Del Camino, SIDEA, Lima, 1996, pp. 20–36.
[5] C. Chácara, F. Zvietcovich, C. Briceño, R. Marques, R. Perucchio, B. Castañeda, S. Uceda, R.R. Morales y Aguilar, On-site investigation and numerical analysis for structural assessment of the archaeological complex of Huaca de la Luna, De 9th International Conference on Structural Analysis of Historical Constructions SAHC2014, Mexico City, 2014.
[6] P.A.H.d.L.L. PHLL, Informe Técnico, Facultad De Ciencias Sociales, Universidad Nacional de Trujillo, 2008, 2016.
[7] L. Binda, A. Saisi, C. Tiraboschi, S. Valle, C.M. Colla y Forde, Application of sonic and radar tests on the piers and walls of the Cathedral of Noto, Constr. Build. Mater. 17 (8) (2003) 613–627.
[8] ASTM D7263, Standard Test Methods for Laboratory Determination of Density (Unit Weight) of Soil Specimens, de ASTM International, West Conshohocken, 2009.
[9] ASTM D4643, Standard Test Method for Determination of Water (Moisture) Content of Soil by Microwave Oven Heating, de ASTM International, West Conshohocken, 2008.
[10] ASTM D422, Standard Test Method for Particle-size Analysis of Soils, de ASTM International, West Conshohocken, 2007.
[11] ASTM D4318, Standard Test Methods for Liquid Limit, Plastic Limit, and Plasticity Index of Soils, de ASTM International, West Conshohocken, 2010.
[12] P.A.H.d.l.L. PHLL, Informe Técnico, Facultad De Ciencias Sociales, Universidad Nacional de Trujillo, 2008.
[13] ASTM D2487, Standard Practice for Classification of Soils for Engineering Purposes (Unified Soil Classification System), de ASTM International, West Conshohocken, PA, 2011.
[14] P. Walker, Australian earth building handbook, Australia, Sydney, 2002.
[15] ASTM C469, Standard Test Method for Static Modulus of Elasticity and Poisson's Ratio of Concrete in Compression, de ASTM International, West Conshohocken, 2014.
[16] J. Almeida, Mechanical characterization of traditional adobe masonry elements, Master Thesis, Guimaraes, 2012.
[17] D. Ciancio, J. Gibbings, Experimental investigation on the compressive strength of cored and molded cement-stabilized rammed earth samples, Constr. Build. Mater. 28 (2012) 294–304.
[18] GOM mbH, ARAMIS User Information Hardware, Brauncshweig, Germany, 2010.
[19] RILEM, CPC 6 tension by splitting of concrete specimen, RILEM Technical Recommendations for the Testing and Use of Construction Materials, (1994) .
[20] D. Oliveira, H. Varum, R. Silva, H. Pereira, P. Lourenço, A. Costa, Caracterização experimental do comportamento diferido de alvenaria de adobe, De Proceedings of the 'V Seminário De Arquitectura Em Terra Em Portugal', Aveiro, 2007.
[21] UNE-EN 1052-1, Métodos De Ensayo Para Albañilería. Parte 1: Determinación De La Resistencia a Compresión, (1999) .
[22] D. Silveira, H. Varum, A. Costa, Influence of the testing procedures in the mechanical characterization of adobe bricks, Constr. Build. Mater. 40 (2013) 719–728.
[23] Popovics, Numerical approach to the complete stress–strain curve of concrete, Cem. Concr. Res. 3 (5) (1973) 583–599.
[24] ASTM C293, Standard Test Method for Flexural Strength of Concrete (Using Simple Beam With Center-Point Loading), de ASTM International, West Conshohocken, 2016.